Amylose–Iodine Complex. I. Sedimentation Behavior[1]

F. R. Dintzis,* A. C. Beckwith, G. E. Babcock, and R. Tobin

Northern Regional Research Laboratory, Agricultural Research Service, U.S. Department of Agriculture, Peoria, Illinois 61604. *Received May 8, 1975*

ABSTRACT: Sedimentation measurements are reported on solutions of blue amylose–iodine complexes in the range of 0.001 to 0.007% amylose. Amylose fractions B and F_2, of weight average molecular weight 4.0×10^5 and 3.4×10^4, respectively, were used in this study. Iodine complexes of these fractions formed polydisperse solutions of limited solubility and stability. Sedimentation coefficients increased as a function of potassium iodide concentration. Values for fraction B complexes varied from $(16.3 \pm 1.0) \times 10^{-13}$ at 1.2×10^{-3} M KI to $(57.2 \pm 7.5) \times 10^{-13}$ at 8.3×10^{-3} M KI; values for fraction F_2 complexes varied from $(10.0 \pm 1.2) \times 10^{-13}$ at 1.2×10^{-13} M KI to $(24.8 \pm 3.9) \times 10^{-13}$ at 9.5×10^{-3} M KI. At constant potassium iodide concentration, sedimentation coefficients, within our experimental error of 10 to 15% standard deviation, are independent of amylose concentration. Time dependence of sedimentation coefficient values was observed for solutions either saturated or unsaturated with respect to the iodine-binding capacity of amylose. For iodine-saturated complex solutions, sedimentation coefficients extrapolated to zero potassium iodide concentration were two to three times greater than for the parent amylose. Measurements are evaluated in terms of possible polyelectrolytic charge effects and aggregation. Under conditions used in these experiments, aggregation of amylose–iodide complexes appears to be the mechanism responsible for the large increase in sedimentation coefficients.

Many properties of the blue complex of amylose–iodine–iodide (AI) are now well established.[2] However, the complex has a tendency to precipitate from aqueous solution at concentrations greater than 0.01%. This behavior has limited experimental measurements of sedimentation coefficients, s, weight average molecular weights, $\bar{M}_w$, and conformations in aqueous solutions. It is now possible to measure some effective mass properties of the AI complex in very dilute solutions with commercially available instrumentation. We examined the sedimentation behavior of AI complexes measured in an analytical ultracentrifuge using absorption optics.

Amylose in aqueous solution has a tendency toward aggregation, reversion to a water-insoluble form, and eventual precipitation. This reversion phenomenon to a water-insoluble form is called retrogradation. The botanical source and chain length of amylose are factors that influence rates of retrogradation.[3,4] Behavior of the AI complex in solution in some ways is similar to that of amylose since both exhibit marginal stability in aqueous solutions at room temperature (ca. 25 °C). Limited solubility and aggregation of the complex have been emphasized by Foster and Zucker.[5] Foster and Paschall[6] also attributed changes in the absorption spectrum of the AI complex to aggregation. Earlier, Meyer and Bernfeld[7] postulated that iodine adsorption occurred on amylose micelles in solution.

Conflicting views exist at present as to the solution state of the AI complex. On the basis of salt effects and calorimetric studies, Ono and co-workers[8,9] postulate AI aggregates in solution. After working with synthetic amyloses produced from glucose 1-phosphate reacting with potato phosphorylase, Pfannemüller et al.[10] state that "association" may occur with AI complexes of degrees of polymerization, $\bar{P}_n$, from about 50 to 80. However, for greater chain lengths they believe there is no evidence of aggregation. Their work has led them to consider a wormlike helical chain to be an adequate model for the AI complex in solution. Senior and Hamori[11] showed that the intrinsic viscosity of amylose solutions decreases significantly upon complex formation with iodine, and they attribute this result to "a shortening of the linear dimension of the polymer chain". They consider their solutions to be free of AI aggregates at the low amylose and iodine concentrations used.

We measured sedimentation properties of solutions containing 0.001 to 0.007% amylose and found that aggregation is the phenomenon most likely to explain our results. High sedimentation coefficients were measured both in solutions saturated and unsaturated with respect to the iodine-binding capacity of amylose. Sedimentation coefficients measured in solutions saturated with respect to the iodine-binding capacity of amylose depend upon KI concentration in solution. Under the conditions we used the simple theory of polyelectrolytic behavior for nonaggregating systems does not explain our results.

Theory

Sedimentation behavior of polyelectrolytes has been treated by Pedersen,[12] Mijnlieff,[13] and Alexandrowicz and Daniel.[14] The Svedberg–Pedersen concept is followed here wherein the actual velocity of an ion consists of a sedimentation velocity achieved under the influence of an isolated applied centrifugal field, $\omega^2 x$, and an electrophoretic velocity obtained by isolated action of an internally created electrical field, $d\psi/dx$. The velocity of each ion is multiplied by its corresponding charge and concentration. The products are then added to obtain the condition of electroneutrality, from which one obtains an expression for $d\psi/dx$. This expression is substituted back into the velocity equation for the macroion. The result is expressed in the notation of Alexandrowicz and Daniel:[14]

$$S_{p'}^* = V_{p'}/\omega^2 x = \bar{M}_{p'}/f_{p'} - [(q_{p'}/f_{p'})\Sigma q_i m_i \bar{M}_i]/[f_i/\Sigma q_i^2 m_i/f_i] \quad (1)$$

where $S_{p'}^*$ = observed sedimentation coefficient of macroion, i.e., the AI complex assumed to be negatively charged; $V_{p'}$ = actual velocity of macroion, which here is considered to be a polyion, noted by subscript, p; ω = angular velocity; x = distance from center of rotation; $\bar{M}_i$ = bouyant weight of ion = $M_i(1 - \bar{v}_i\rho)$; M_i = mass of ion; $\bar{v}_i$ = partial specific volume of ion; ρ = solution density; f_i = frictional coefficient of ion; m_i = concentration of free ions in moles per milliliter; and q_i = charge on ion.

The term $\bar{M}_{p'}/f_{p'}$ is considered as the sedimentation coefficient, $S_{p'}$, of the charged macroion uncorrected for effects of the internally generated field. The denominator term, $\Sigma q_i^2 m_i/f_i$, is equivalent to $\Sigma q_i m_i u_i$, where u_i is the electrophoretic mobility, and the summation represents solution specific conductivity, K. Pedersen[12] points out in his comments on the primary salt effect the quantity, $S_{p'} - S_{p'}^*$, in the first approximation should vary linearly with $1/K$. According to eq 1, $S_{p'}^*$ depends upon both macroion and salt concentration.

Equation 1 may be rewritten by placing both terms in the numerator and factoring out of the summations the macroion terms which cancel:

$$S_{p'}^* = \frac{S_{p'}\Sigma m_i/f_i - (Z_{p'}/f_{p'})\Sigma q_i m_i s_i}{(Z_{p'}^2 m_p/f_{p'}) + \Sigma m_i/f_i} \quad (2)$$

where $Z_{p'}$ = net charge on macroion; and s_i = sedimentation coefficients of small ions. Under the conditions of these experiments (see Appendix) we can show that since the denominator term in $Z_{p'}^2$ is small, compared to $1/f_{i'}$, eq 2 becomes:

$$S_{p'}^* \sim S_{p'} - \frac{Z_{p'}[s_{K^+} + s_{I^-}]}{f_{p'}[(1/f_{K^+}) + (1/f_{I^-})]} \quad (3)$$

The relative concentration of KI in these experiments is considered to be sufficiently high that concentrations of all other small ions are neglected. By using numerical estimates, presented in the Appendix, for AI complexes of amylose fraction F_2, eq 3 becomes:

$$S_{p'}^* \sim \frac{1.3nM_A}{f_{p'}N}[(1 - \bar{v}\rho) - 18 \times 10^{-3}\theta] \quad (4)$$

where n is the number of AI chains which may associate to form an aggregate. According to this estimate, the θ term, which represents the retarding force generated by charge effects, is at most only 5% of $(1 - \bar{v}\rho)$, which is of the order of 0.4. Thus, eq 4 shows the main source of $S_{p'}^*$ variation could be the quantity, n, which could vary with KI concentration and would represent aggregation.

Alexandrowicz and Daniel[14] have modified the Svedberg–Pedersen equation by explicitly introducing a term to allow for changes in the frictional coefficient due to nonelectrostatic interactions. Their eq 9 (ref 14) may be considered to describe $(1/S_{p'}^*)$ in terms of two parameters: polyion concentration and polyion concentration divided by salt concentration. When applied to our AI complex system, their eq 9 becomes (see Appendix):

$$(S_{p'}^*)^{-1} \sim (S_{p'}^0)^{-1} + B_1C_A + B_2(C_A/m_{KI}) \quad (5)$$

Both eq 4 and 5 will be considered later in terms of measurements made on AI complexes.

Experimental Section

Amylose was isolated at the Northern Laboratory from dent maize starch and recrystallized twice as the 1-butanol complex.[15] Fractions from dent maize amylose were obtained by ethanol precipitation from methyl sulfoxide.[16] Fractions B and F_2, with $\bar{M}_w$ of 4.0×10^5 and 3.4×10^4, respectively, were used in our work. These fractions were obtained from two 25-g amylose samples, batch 1 and batch 2. Fractions 3 and 4 from batch 1 were combined with fraction 4 from batch 2 and refractionated into fractions B and C. The lowest molecular weight fractions, fraction 7 from batch 1 and fraction 6 from batch 2, were combined and refractionated into fractions F_1 and F_2. Stock solutions of the two fractions, B and F_2 containing about 1.6% amylose in 95% methyl sulfoxide–5% H_2O, were prepared and stored in a freezer. Amylose concentrations were determined by optical rotation on the basis of the specific rotation at the sodium D line $[\alpha]_D$ 189°.[17]

Methyl sulfoxide, supplied by Crown Zellerbach[34] in 50-gal drums, was distilled under vacuum before use. Ultrapure grade I_2 and KI were purchased from Alfa Inorganics and used directly from their glass-stoppered bottles. Sucrose, "Standard Sample", was purchased from the National Bureau of Standards and used directly. A plastic 1-ml syringe, "Plastipak", purchased from Becton-Dickinson, was heated to soften the base. The softened base was pulled out to form a small diameter tube attached to the syringe barrel. This modified nonmetal syringe served to transfer AI solutions into centrifuge cells.

The AI preparations were quite sensitive to destabilization by ionic contaminants. Trace amounts of acid, base, or salts seemed to cause eventual precipitation of the blue complex. For this reason unbuffered solutions were used that had a pH range of 5.5 to 6.8. Since contact with such metals as copper, aluminum, or stainless steel could cause precipitation, AI solutions were prepared with ceramic spatulas and stored in thoroughly cleaned and rinsed glassware. According to constant absorbancy measurements at 546 nm, some AI solutions stored in glass-stoppered flasks at room temperature have remained stable for at least a year.

A primary I_2–KI stock solution was prepared by dissolving 0.1 g I_2 and 2.0 g KI into 25 ml of redistilled water. This solution was filtered through a sintered glass filter. Secondary solutions were made from the primary stock at a fivefold dilution.

The first step in making an AI complex solution was to weigh 2% sucrose, weight/volume, into a glass-stoppered flask. Sucrose is used to help stabilize the sedimenting gradient. About 90% of the necessary volume of redistilled water was added. Then, 25λ amylose stock solution and 0.40 ml of secondary I_2–KI stock solution were added. The flask was swirled after addition of each reagent and then made to final volume by weight. All AI complex and I_2–KI stock solutions were stored in the dark in aluminum foil-wrapped glass-stoppered flasks.

A reference series of AI complex solutions, Y, was prepared to contain initial weight ratios of amylose–I_2–KI of 1.0:0.79:20. For amylose fraction F_2, two other series, X and Z, were prepared that contained, respectively, one-half or twice the quantity of I_2 and KI. Amylose concentration was changed by changing volume of the final solution. As a consequence, the KI concentration in these solutions was a function of amylose content.

Some studies were made on AI complex solutions of amylose fraction B at constant KI concentration. Separate secondary stock solutions of I_2–KI were prepared with amounts of KI necessary to maintain a constant KI concentration throughout the range of 0.001 to 0.007% amylose. The ratio of amylose–I_2–KI for 0.003% amylose solutions was chosen to be the same as for series Y. Hence in these constant KI concentration AI complex solutions a ratio of amylose–I_2 was maintained at 1.0:0.79 while the ratio of amylose–KI was a function of amylose concentration. All AI complex solutions of 0.003% amylose were prepared to a final volume of 14.0 ml and contained: 0.28 g of sucrose, 4.2×10^{-4} g of amylose, 3.3×10^{-4} g of I_2, and 84×10^{-4} g of KI (3.6×10^{-3} M KI).

Iodine binding studies were done using a differential, potentiometric iodine titration apparatus and technique similar to that of Banks, Greenwood, and Muir.[18] Measurements were made at about 25 °C on solutions containing amylose, DMSO, and KI at concentrations used in sedimentation runs. Constant KI concentration was maintained during iodine binding measurements.

AI complex solutions saturated with respect to the iodine-binding capacity of amylose followed Beers law so that amylose concentrations were verified by absorbancy measurements at 546 nm.

Sedimentation runs were made in a Spinco Model E ultracentrifuge equipped with a photoelectric absorption scanner. Details of this equipment have been reported previously.[19] Double sector, 6-mm, Epon resin cell centerpieces or 12-mm double sector Epon resin or Kel F centerpieces were used also. Absorbance was monitored at either 546 or 590 nm. The AI complex was sedimented at 25 °C and speeds between 10 000 and 24 000 rpm.

Rotors had either a three- or five-cell capacity plus one position for the reference counterweight. At least five or six measurements were attempted on a given AI preparation. Two consecutive sedimentation runs were made with the three-cell capacity rotor, and occasionally, one cell was shaken after the first run to mix its contents thoroughly for which s was measured again during the second run. An average of four valid s measurements were obtained on each AI solution, and usually two AI preparations were used for each amylose concentration.

The electrical signal proportional to solution concentration was punched on paper tape for processing and computation on an IBM-1130 computer. Absorbance of the AI complex in the centrifuge cell was measured at medium scan rates of approximately 0.022 cm/s. The signal was digitized at a rate of 8 samples/s. This digitizing rate yielded sample points across the liquid column at radial increments, Δr, of 0.0027 cm. Cells were filled about three-quarters full so that approximately 350 measurements were taken across the solution during a normal run.

Data Processing. Relationships between the sedimentation coefficient of uncharged molecules, s, and some solution properties of such molecules are well established and available in textbooks.[20] Excellent review articles describing both theory and practice are available.[21,22] Goldberg[23] firmly established that the boundary position of sedimenting material should be calculated as a square root of the second moment about the center of rotation. The distance from the center of rotation to the sedimenting boundary, $\bar{r}$, is defined by the relation:

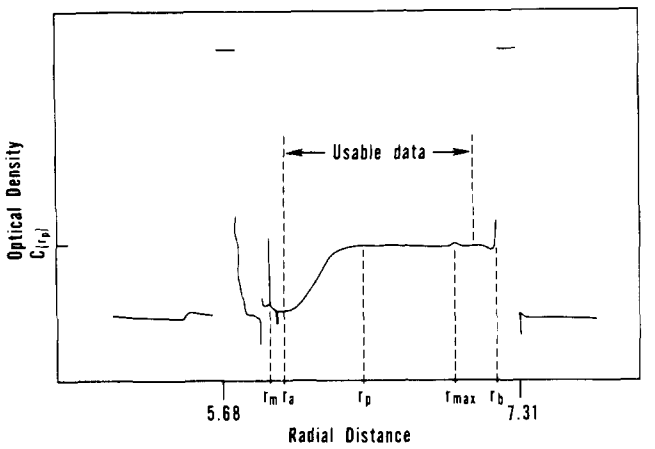

Figure 1. Absorption scan trace of 0.001% fraction B amylose–iodine–iodide (AI) complex at 590 nm, constant KI series, after about 20 min at 12 000 rpm and then about 28 min at 24 000 rpm. See text for definition of symbols.

$$\bar{r}^2 = \int_{r_a}^{r_p} r^2(\partial C/\partial r)\,dr \Big/ \int_{r_a}^{r_p} (\partial C/\partial r)\,dr \qquad (6)$$

where C is the volume concentration of sedimenting material; r_p is the distance from center of rotation to a "plateau" region between $\bar{r}$ and the cell bottom where initially $\partial C/\partial r = 0$; and r_a is the distance from the center of rotation, past the depleted meniscus whose position is, r_m, to the region where initially $\partial C/\partial r \cong 0$.

In this work C may be taken to represent a count number that is the output result of light absorption by the AI complex and the optical and electrical constants of instrumentation. All AI species in solution are assumed to have the same absorption coefficients, which are independent of concentration and pressure.

The numerator of eq 6 may be integrated by parts. The denominator then becomes $C_{(r_p)} - C_{(r_a)}$ and the results are combined with application of the trapezoidal approximation to yield:[21]

$$\bar{r}^2 = \frac{r_p^2 C_{(r_p)} - r_a^2 C_{(r_a)} - \Delta r \sum_{i=1}^{n-1} [r_i C_{(r_i)} + r_{i+1} C_{(r_{i+1})}]}{C_{(r_p)} - C_{(r_a)}} \qquad (7)$$

where $C_{(r_i)}$ = count value at radial distance, r_i and $dr \cong \Delta r$. Radial positions are calculated by the relation:

$$r_j = r_m + (j - 1)\Delta r \qquad (8)$$

Equation 7 is convenient for computer calculations.

A computer program was written to consider "usable" data obtained from an absorbance scan.[19] A scan trace from a typical well behaved sedimentation run is shown in Figure 1. Measurement anomalies near the meniscus are rejected as well as high absorptions caused by sedimented material or anomalies at the cell bottom. The radial position, r_{max}, of the maximum count value in usable raw data is found. This position becomes a limit for data processing. The midpoint of an interval of the AI concentration function containing 37 data points, starting at the position chosen near the meniscus, is smoothed by fitting it to a cubic equation.[24] The 37 data-point interval is then advanced to the next measurement point toward the cell bottom and again the midpoint smoothed. This process is continued until position r_{max} is reached. Signal noise content is greatly reduced by the smoothing process.

The cubic equation is also used to extrapolate smoothed data to r_m and the cell bottom position, r_b, as well as to evaluate $\partial C/\partial r$ across the liquid column. If a derivative maximum is found in the smoothed data, its position, $r_{d,max}$, is printed out. If beyond $r_{d,max}$ $\partial C/\partial r \sim 0$, then the position at which this occurs is taken as r_p and the associated smoothed count value is taken as $C_{(r_p)}$. Only if $\partial C/\partial r \cong 0$ at $r = r_m$ is $(\bar{r}^2)^{1/2}$ calculated. The radial position, $r_{(1/2)C}$, at which $C_{(r_i)} = \frac{1}{2}C_{(r\,max)}$ is found and recorded. Three parameters of the sedimenting boundary position are calculated and printed out: $(\bar{r}^2)^{1/2}$, $r_{d,max}$, and $r_{(1/2)C}$. Ideal behavior of a monodisperse material would be represented by equal values of these three parameters.

Values of s are calculated from the slope of a plot of $\ln \bar{r}$ vs. time and are extrapolated to obtain an infinite dilution value, s^0, by a plot of $1/s$ vs. amylose concentration.[21]

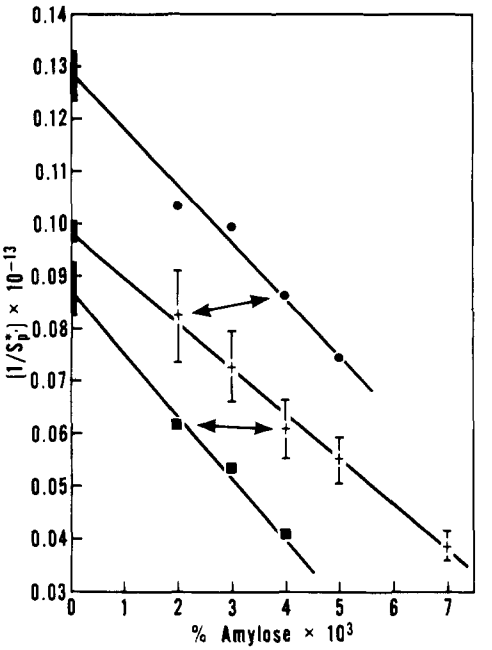

Figure 2. Sedimentation behavior of AI complexes of fraction F_2 amylose. Standard deviations in $1/S_{p'}^*$ are indicated for series Y. Standard deviations in apparent $1/S_{p'}^{0*}$ at zero amylose concentration are indicated by darkened bands on $1/S_{p'}^*$ axis. $S_{p'}^{0*}$ = sedimentation coefficient of AI complex ion at zero amylose concentration and zero KI concentration. Arrows show data at equal [KI]: upper arrows, 2.4×10^{-3} M KI; lower arrows, 4.7×10^{-3} M KI. (●) Series X, constant weight ratios of amylose–I_2–KI of 1:0.395:10; (+) series Y, constant weight ratios of amylose–I_2–KI of 1:0.79:20; (■) series Z, constant weight ratios of amylose–I_2–KI of 1:1.58:40.

Table I
Series Y Data

Nominal amylose concn, %	No. of $S_{p'}^*$ measurements	$(1/S_{p'}^*) \times 10^{-13}$	No. of AI preparations
0.002	19	0.0820 ± 0.0090	3
0.003	10	0.0724 ± 0.0070	2
0.004	13	0.0608 ± 0.0054	2
0.005	18	0.0556 ± 0.0042	2
0.007	12	0.0389 ± 0.0032	2

Results

Measurements of $S_{p'}^*$ presented here are those calculated from $(\bar{r}^2)^{1/2}$. This parameter, in addition to being the proper one to use for a heterogeneous system, seemed to be less susceptible to instrumentation noise and yielded more consistent sets of $S_{p'}^*$ values. In most instances values of $S_{p'}^*$ calculated from $(\bar{r}^2)^{1/2}$ were at least 10% greater than $S_{p'}^*$ values calculated from $r_{d,max}$ or $r_{(1/2)C}$. This result verifies heterogeneity of the sedimenting complex.

Reciprocal sedimentation coefficients of AI complex solutions of fraction F_2 amylose, as a function of amylose concentration, are shown in Figure 2. These solutions are saturated with respect to the iodine-binding capacity of amylose. Each $1/S_{p'}^*$ value displayed is an average of at least ten measurements on two different solutions. Standard deviations in $1/S_{p'}^*$ are indicated for series Y solutions. Lines extrapolated to zero amylose concentration represent the least-squares fit to all data of a series. Solutions at equal KI concentrations are noted by arrows. Details of series Y data are presented in Table I.

Sedimentation behavior of AI complexes of fraction B is

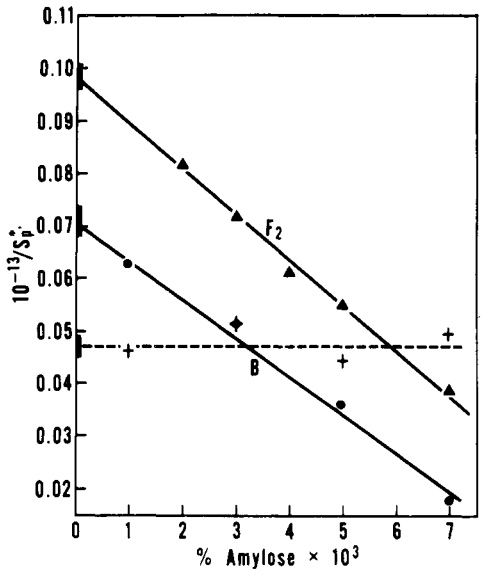

Figure 3. Sedimentation behavior of AI complexes: (▲) F_2 amylose, series Y; (●) B amylose, series Y, solid line; (+) B amylose, constant KI, dashed line. Standard deviations in apparent $1/S_{p'}^{0*}$ indicated by dark bands on $1/S_{p'}^*$ axis. Solid lines in this figure (and Figure 2) represent $1/S_{p'}^*$ variation with both amylose and KI concentrations.

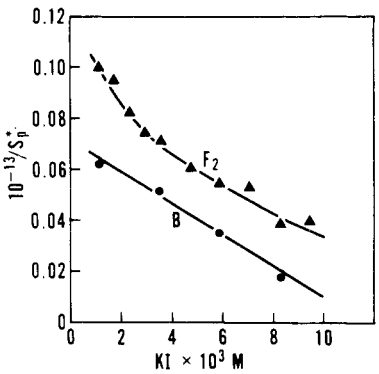

Figure 4. Reciprocal sedimentation coefficient behavior as a function of [KI]. Points represent average values: F_2, fraction F_2 AI complex; B, fraction B AI complex.

represented in Figure 3 by the two lines (dashed and solid) labeled B. The dashed line is the least-squares fit to data obtained from solutions of constant KI concentration (i.e., 3.6×10^{-3} M KI). The solid B line represents the least-squares fit to data obtained from series Y solutions. For comparison, the corresponding series Y data for AI complexes of fraction F_2 are plotted by line F_2. Series Y concentrations greater than 0.007% amylose and series Z concentrations greater than 0.004% amylose were unstable if sedimentation was measured at rotation rates used in these experiments (i.e., ≥ 10 000 rpm). Such AI solutions either yielded large and imprecise s values or exhibited insoluble precipitates in the ultracentrifuge cell bottom after a run.

Sedimentation data are plotted as a function of KI concentration in Figure 4. Average values are plotted as a function of KI concentration. Reciporcal sedimentation coefficients of fraction B AI complexes are a linear function of KI concentration over the limited range of measurements, whereas reciprocal sedimentation coefficients of fraction F_2 AI complexes are not.

All data from AI complexes of fraction F_2 (Figure 2) are replotted in Figure 5 in terms of the parameters of eq 5.

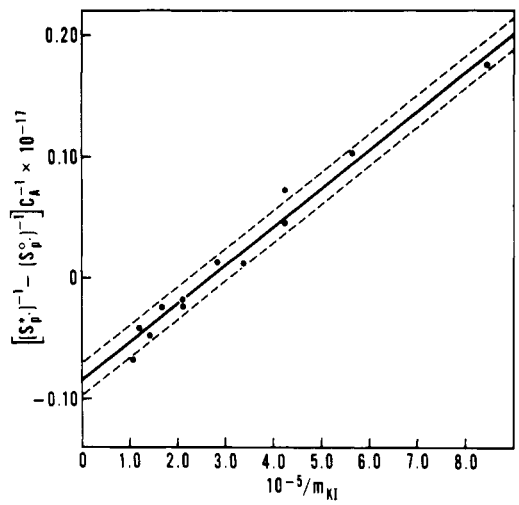

Figure 5. Sedimentation data of AI complexes of fraction F_2 amylose plotted according to the parameters of eq 5 (see text). Dashed lines represent standard deviation of data. C_A in g of amylose/ml, m_{KI} in mol/ml. Data analysis yields the results: $(S_{p'}^0)^{-1} = 6.8 \times 10^{11}$; $B_1 = -8.5 \times 10^{15}$; $B_2 = 3.2 \times 10^{10}$.

The data are fitted to a straight line by a regression analysis. Thus the three lines in Figure 2 are reduced to a single function in both Figures 4 and 5.

A time dependence of $S_{p'}^*$ was noted in this work. Sometimes 3 days were needed to reach an apparent equilibrium $S_{p'}^*$ value, though sometimes 1 day was sufficient. Time dependence of $S_{p'}^*$ values for AI complex solutions saturated with respect to iodine-binding capacity of amylose is shown in Table II.

Concern about solution stability and time-dependent behavior led to additional investigation. Blue complex absorption at 610 nm and I_3^- absorptions at both 352 and 288 nm were monitored as a function of time[24] (Figure 6). Absorption of the AI complex is stable, whereas that of I_3^- decreases with time. Absorption by I_3^- also decreased with time in controls that contained either only sucrose and I_2–KI or only sucrose, methyl sulfoxide, and I_2–KI.

Measurements were made on AI solutions not saturated with respect to the iodine-binding capacity of amylose. Sedimentation coefficients are tabulated in Table III. Time dependence of $S_{p'}^*$ again is observed. Because I_3^- in solution decreases with time, values of the ratio (wt of I_2 added/wt of I_2 bound at saturation) in solution are actually lower than initial values reported in the tables. Absorption measurements at 590 nm on I_2-unsaturated AI solutions stored 6 days under N_2 showed that intensity of the blue decreased with time.

Results of iodine-binding measurements on amylose fractions are presented in Table IV.

Table V summarizes $S_{p'}^*$ measured at lowest KI concentrations, apparent $S_{p'}^{0*}$, and s^0 values obtained from measurements on aged AI complex solutions saturated with respect to iodine-binding capacity of amylose and solutions of parent amylose. Individual cell measurements were fitted to a least-squares analysis to obtain extrapolated values. For AI complexes of fraction F_2, apparent $S_{p'}^{0*}$ was evaluated from $1/S_{p'}^*$ vs. $[KI]^{1/2}$ to reduce uncertainty in extrapolating caused by the curvature shown in Figure 4. The large increase in sedimentation coefficient values of iodine-complexed amylose is obvious.

Discussion

Treatment of data in Figure 2 by least-squares analysis shows a family of three lines with statistically parallel

Table II
Time Dependence of $S_{p'}$*

Solution	Wt of I_2 added[a] / wt of I_2 bound at saturation	No. of $S_{p'}$* values	Solution age	$S_{p'}$* × 10^{13}
	Amylose Fraction F_2			
0.003%, series X	2.3	7	3–6 hr	9.2 ± 1.1
		5	2 days	11.4 ± 1.6
		4	5 days	11.3 ± 0.9
0.003%, series Y	4.4	5	2–6 hr	11.9 ± 0.5
		4	10 days	14.7 ± 1.0
0.004%, series Y	4.4	5	2–6 hr	10.0 ± 3.1
		6	1 day	14.9 ± 3.7
		3	4 days	17.1 ± 1.1
		6	11 days	17.2 ± 1.1
	Amylose Fraction B			
0.003%, series Y	4.0	4	2–6 hr	14.3 ± 1.6
		6	10 days	19.3 ± 1.5

[a] Calculated on the assumption of an I_2 binding of 19.5 and 17.5 mg of I_2/100 mg amylose for fractions B and F_2, respectively.

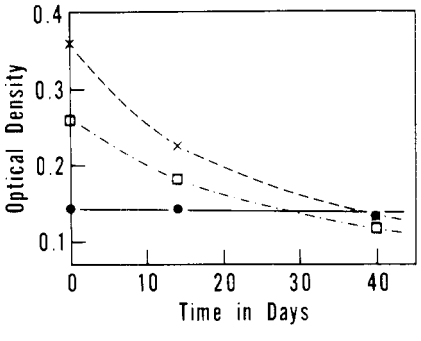

Figure 6. Time dependence for absorptions of 0.003% F_2 AI complex, series Y (●), and I_3^- (□, x) in 0.20-cm cell vs. blank containing 2% sucrose, 25λ methyl sulfoxide, and 0.003% amylose at a standard final volume of 14.0 ml: (●) 610 nm; (□) 352 nm; (×) 288 nm.

slopes. The data also demonstrate significantly different $S_{p'}$* values calculated at a mean concentration of 0.003% amylose, where the confidence level is greatest. Solutions at equal KI concentrations (arrows) yield the same sedimentation coefficient values within experimental error.

Solid line B (Figure 3) has a slope about 15% less than that of line F_2. The two different amylose fractions yield AI complexes that exhibit similar sedimentation behavior, and the higher molecular weight fraction yields AI complexes that have larger sedimentation coefficients. Dashed line B (Figure 3) shows that at constant KI concentration the sedimentation coefficient of the AI complex is independent of amylose concentration. Inspection of Figures 2 and 3 indicates that sedimentation behavior of the AI complex depends upon molecular weight of the parent amylose and KI concentration and suggests that $S_{p'}$* values are independent of amylose concentration.

By graphing $1/S_{p'}$* values vs. KI concentration, the three lines in Figure 2 are transformed to a single function of $1/S_{p'}$* vs. [KI] in Figure 4, line F_2. Fraction B data appear linear when plotted this way. While average ($1/S_{p'}$*) values of fraction B AI complexes vs. [KI] are a linear function over a limited KI concentration range, it is possible that curvature would be exhibited if measurements were made at lower salt concentrations. The great increase in $S_{p'}$* values at KI concentrations greater than 0.01 M (as precipitation becomes evident in the ultracentrifuge cell) implies that the two lines in Figure 4 might have a general sigmoid shape. Alternatively, the curvature exhibited by AI complexes of fraction F_2 may signify a real difference in solution properties from those of AI complexes of fraction B.

Failure to describe $S_{p'}$* variation quantitatively is a known difficulty with the basic Svedberg–Pederson model of polyelectrolytic behavior with respect to the "primary charge effect". However, according to our estimates this model says the primary charge effect in our experiments is neglible (see Appendix). We have incorporated an aggregation number, n, into eq 4 to account for aggregation being the mechanism by which $S_{p'}$* would increase. If n were a

Table III
I_2-Unsaturated AI Complex Solutions

Solution (0.004%)	Wt. of I_2 added[a] / wt of I_2 bound at saturation	No. of $S_{p'}$* values	Solution age	$S_{p'}$* × 10^{13}	$(1/S_{p'}$*) × 10^{-13}
		Amylose Fraction F_2			
0.90 × 10^{-3} M KI	0.85	5	7 days	18.8 ± 3.1	0.053
		Amylose Fraction B			
0.87 × 10^{-3} M KI	0.74	6	7 days	23.2 ± 2.7	0.043
0.87 × 10^{-3} M KI	0.74	6	2–6 hr	23.2 ± 2.3	0.043
0.82 × 10^{-3} M KI	0.69	6	2–6 hr	16.7 ± 1.2	0.060
		4	7 days	20.9 ± 0.8	0.048
		2	7 days	30.7 ± 1.5	0.033

[a] Calculated on the assumption of an I_2 binding of 19.5 and 17.5 mg of I_2/100 mg of amylose for fractions B and F_2, respectively.

Table IV
Iodine Binding Measurements

Amylose type	% amylose	KI concn, 10^3 M KI	Mg of I_2 bound/100 mg amylose
Dent corn, unfractionated	0.001	1.2	19.5
	0.001	3.6	19.4
Fraction B	0.001	1.2	19.1
	0.003	3.6	19.5
Fraction F_2	0.002	1.2	17.4
	0.002	3.6	17.7

[a] Titrations done at constant KI concentration at 25 ± 1 °C.

Table V
Sedimentation Coefficients of AI Complexes

Fraction	% amylose	$S_{p'}^* \times 10^{13}$
A. Measured at Lowest KI Concentration of 1.18×10^{-3} M		
F_2	0.002	9.98 ± 1.18
B	0.001	16.3 ± 0.96
B. Extrapolated to Zero KI Concentration		Apparent $S_{p'}^{0*}$ or $s^0 \times 10^{13}$
F_2		
Extrapolated from $1/S_{p'}^*$ vs. $KI^{1/2}$ (Figure 4)		7.38 ± 0.15
Amylose in H_2O[a]		2.5 ± 0.2[b]
B		
Extrapolated from $1/S_{p'}^*$ vs. KI (Figure 4)		14.0 ± 0.9
Constant KI concentration, 3.6×10^{-3} M, extrapolated from $1/S_{p'}^*$ vs. % amylose (Figure 3)		21.3 ± 1.9
Amylose in H_2O		6.84 ± 0.20[b]

[a] Measured in 95% methyl sulfoxide–5% H_2O solvent and corrected to H_2O by a standard formula for solution viscosity changes, assuming no conformation change and that the same partial specific volume in both solvents equals 0.6. [b] Distance measured from center of rotation to maximum peak height of the schlerien patterns.

function of KI concentration, eq 4 would qualitatively describe our results (Figure 4).

In their modification of the Svedberg–Pederson concept Alexandrowicz and Daniel[14] introduced polymer concentration to account for concentration dependence effects between polyions. Their equation applied to our AI complexes (eq 5) has the interesting property of fitting our F_2 data in a formal manner (Figure 5). Numbers obtained from Figure 5 do not agree with experimental results. The data slope value leads to an estimate of $\theta > 1$ (see Appendix) and regression analysis yields an estimated value of $S_{p'}^{0*}$ ($\sim 15 \times 10^{-13}$) which is twice as large as the experimentally estimated value of 7.4×10^{-13} (Table V). In addition our results indicate $S_{p'}^*$ is independent of C_A (Figure 2, arrows, and Figure 3, dashed line) while eq 5 shows C_A as a variable. These results are not surprising, for eq 5 was designed for nonaggregating systems. The point is that an equation of the form of eq 5, containing KI concentration, does fit our results.

Sedimentation data alone do not allow separation of possible polyelectrolytic charge effects from possible aggregation phenomena. (However, another report will be made on molecular weight measurements of these AI complexes that will prove aggregation is a major cause of observed $S_{p'}^*$ behavior.) If n increases as KI concentration increases, the large variation in $S_{p'}^*$ would be explained. This postulate seems to be supported by experimental observations here in which series Y solutions, greater than 0.007% amylose, and series Z solutions, greater than 0.004% amylose, tend to precipitate during an ultracentrifugation run. If this explanation is correct, then results in Figure 4 (and Figure 5) represent aggregation and incipient "salting out" of the AI complex as KI concentration increases.

Possible similarity of Figure 4 to data obtained from salting-out experiments should be mentioned.[27] In such experiments linear data are fitted by an empirical equation: $\log (A/A^0) = mK_s$, where A is solubility of solute in aqueous salt solution, A^0 is corresponding solubility in pure water, m is salt molality or ionic strength of the solution, and K_s is a salting out constant. Similar thermodynamic interpretation of salting out would apply to the AI complex system. As KI concentration increases, the activity coefficient of an AI complex n-mer in solution is increased until the n-mer associates. Continued increase in KI concentration causes further association and increased particle mass until a critical region is entered and precipitation (possibly time dependent) occurs. By this reasoning ($1/S_{p'}^*$) would be proportional to $\log A/A^0$, and Figure 4 would indicate that the AI complex is salted out by KI at a concentration about two orders of magnitude less than is required for other salts to salt out proteins or ethyl acetate.

Examination of the most reliable "aged solution" $S_{p'}^*$ values, in Table II, reveals increases of 18 to 26% over "fresh solution" values. Although reasons for these increases are unknown, one may speculate they may be caused by association of chains of AI complexes to form an aggregate in which either, or both, n and aggregate shape may reach an equilibrium value. Also, $S_{p'}^*$ would increase if the final charge, $Z_{p'}$, on the aggregate were to decrease from an initial higher formation value. Approximately an hour is required to perform a sedimentation run. Because of this time lag, increases in $S_{p'}^*$ reported here are probably an unknown fraction of the actual increase taking place in solution.

Examination of Table III reveals that aged AI complex solutions unsaturated with respect to the iodine-binding capacity of the total amylose in solution exhibit $S_{p'}^*$ values similar to, or greater than, those measured in aged I_2 saturated AI complex solutions when compared on the basis of amylose concentration. On a basis of KI concentration (Figure 4), however, these $S_{p'}^*$ values in Table III are all greater than corresponding values obtained in I_2 saturated solutions (compare with Figure 3). Variation in Table III data is similar to, or perhaps somewhat greater than, variation observed with I_2-saturated AI complexes. For example, two different 0.004% solutions, one fresh and one aged, have the same $S_{p'}^*$ values, whereas two $S_{p'}^*$ values of an aged solution are 30% greater than the other four. For reasons unknown to us, I_2-unsaturated AI complex solutions seem to be more unstable than corresponding I_2-saturated solutions. Observations of time-dependent behavior and high $S_{p'}^*$ values in I_2 unsaturated AI complex solutions may indicate that aggregation occurs also under such conditions. To avoid possible time-dependence effects, all $S_{p'}^*$ measurements reported here were made on solutions less than 4 weeks old.

Measurements reported in Table IV confirm approximately normal iodine binding values for fraction B and unfractionated amylose under conditions of our ultracentrifugation experiments. The value reported for fraction F_2 could represent decreased binding of iodine by amylose chains at the low molecular weight portion of the F_2 distribution. These measurements indicate that DMSO in our AI

complex solutions saturated with respect to the iodine binding capacity of amylose does not interfere with iodine binding. From this we infer that DMSO is not likely to be complexed with amylose in our AI complex solutions.

Loss of I_3^- with time (Figure 6) represents one form of nonequilibrium in AI solutions. This loss does not affect $S_{p'}$* values measured during 2 months on I_2-saturated solutions because they initially contain a large excess of I_3^-. A reduction of 25–30% in bound I_2 causes a drastic reduction in absorbance at 590 nm. This intensity decrease limited the ranges of unsaturated amylose concentrations that could be measured.

Formation of blue color upon addition of I_2–KI to an amylose solution is shown to be a reaction with about a 0.4 s half-life.[28] Addition of I_2 after apparent saturation causes a shift of the AI absorption maximum, λ_{max}, from about 615 nm to perhaps 650 nm. This phenomenon is termed "a second absorption process".[29] Other workers postulate aggregation of partially or completely filled helices to be the most likely process to explain the second adsorption phenomenon.[30] However, $S_{p'}$* time dependence seems not to be associated with the λ_{max} shift. Both I_2-saturated and unsaturated AI complex solutions show time dependence, but λ_{max} shift is observed only in I_2-saturated solutions. A shift in λ_{max} was observed in both fresh and aged I_2 saturated AI complex solutions.

Apparent $S_{p'}^{0}$* values for AI complexes listed in Table V may be interpreted as representing $S_{p'}$* of a macroion near a state of minimum, n, and maximum effective charge.[26] Estimates of apparent $S_{p'}^{0}$* are based on the assumption that it is valid to extrapolate data from Figure 4 in a linear manner to a state of zero KI concentration. We consider the facts that $S_{p'}$* measured at lowest KI concentrations (Table V) are much greater than s^0 of the parent amylose to be strong evidence that the AI complex in solution is an aggregate and that increase in $S_{p'}$* with increase in [KI] represents mainly aggregate growth. However, some $S_{p'}$* variation with [KI] might be caused by changes in aggregate configuration. For example, light-scattering measurements on systems of rodlike poly(γ-benzyl L-glutamate) in helicogenic solvents have been interpreted by Elias and Gerber[32,33] to represent a combination of change in aggregate size and shape. At concentrations of about 10^{-3} g/ml, aggregates (micelles) of closely bunched poly(γ-benzyl L-glutamate) rods are considered to begin to change to a cyclic or ringlike configuration of rods associated end to end as concentration is lowered.

These experiments were done on a material of limited solubility in a system where it is possible that I_2-saturated AI complexes exist in a state of metastable equilibrium. Despite these problems, we believe that our results are valid and that they demonstrate more work is needed before a satisfactory understanding is achieved of AI complex behavior in solution.

Acknowledgment. We thank Dr. W. F. Kwolek, Biometrician, North Central Region, Agricultural Research Service, U.S. Department of Agriculture, stationed at the Northern Laboratory, for assistance with data analysis and Dr. C. H. Chervenka of Spinco Division, Beckman Laboratories, Inc., for his loan of a prototype unfilled Kel-F centrifuge cell and his comments concerning cell materials.

Appendix

Consider the net macroion charge as:

$$Z_{p'} = \theta\nu C_A/r_p = \theta\nu n M_A$$

where θ is the fraction of unbound counterions, K^+, that are free to move independently in solution. For calculation purposes we assume I_3^- is the bound species, though Cronan and Schneider[30] consider the bound species to vary from I_2 to possibly I_4^{2-} as a function of iodide concentration: ν = mol of I_3^- bound/g of amylose, where I_3^- is a result of the reaction $I_2 + I^- \rightarrow I_3^-$; C_A = g of amylose/ml; M_A = molecular weight of amylose; n = number of AI chains which may associate to form an aggregate; m_p = mol of AI complex/ml = C_A/nM_A.

These experiments were run under the following conditions for amylose fraction F_2 (series Y conditions listed):

$$m_{KI} \sim (2\text{–}8) \times 10^{-6} \text{ mol/ml}$$

$$m_p \sim \frac{(2\text{–}7) \times 10^{-9}}{3.4n} \text{ mol/ml}$$

$$m_{I_2} \sim (0.062\text{–}0.22) \times 10^{-6} \text{ mol/ml}$$

$$M_A \sim 3.4 \times 10^4$$

Our F_2 amylose binds about 0.175 g of I_2/g of amylose, therefore $\nu \sim 6.9 \times 10^{-4}$ mol of I_3^- bound/g of amylose and M, the molecular wt of the AI complex, $\sim 1.26nM_A$.

The following sums are obtained from estimates presented by Pedersen:[12]

$$s_{K^+} + s_{I^-} \sim 0.5 \times 10^{-13}$$

$$[(1/f_{K^+}) + (1/f_{I^-})] \sim 10^9$$

$f_{p'}$, the fractional coefficient of the AI complex ion, is calculated from a standard definition of sedimentation coefficient:

$$S_{p'}^* = \frac{M(1 - \bar{v}\rho)}{Nf_{p'}} \sim \frac{1.3nM_A(1 - \bar{v}\rho)}{Nf_{p'}}$$

where N is Avagadro's number.

M is estimated to be $\sim 3 \times 10^5$. This estimate and reagent concentrations chosen below are based on sedimentation equilibrium measurements reported in paper II.

Density of the AI complex is taken as ~ 1.7 g/cm^3, the solid state estimate.[31] Hence, the term $(1 - \bar{v}\rho)$ is taken as $(1 - 1/1.7) \sim 0.4$. At KI = 2.4×10^{-3} M, $S_{p'}^* \sim 12.5 \times 10^{-13}$ (Figure 4) and therefore,

$$f_{p'} \sim 1.6 \times 10^{-7}$$

The relations $m_{K^+} \sim m_{I^-} = m_{KI}$ are assumed to be valid. These estimates and approximations yield the results:

$$Z_{p'}^2 m_p/f_{p'} \sim 14\theta^2$$

$$10^3 \sim <\Sigma m_i/f_i \sim <10^4$$

$$i = K^+, I^-$$

where $0 < \theta < 1$ (by definition) and we let $C_A \sim 2 \times 10^{-5}$ g/ml.

Substitution of numerical estimates into eq 3 yields:

$$S_{p'}^* \sim \frac{1.3nM_A}{f_{p'}N}[(1 - \bar{v}\rho) - 18 \times 10^{-3}\theta] \qquad (4)$$

where $Z_{p'}$ is assumed to be negative.

Equation 9 of Alexandrowicz and Daniel[14] may be written for these AI complex measurements as:

$$(S_{p'}^*)^{-1} = (S_{p'}^0)^{-1}(1 + 1.3C_AK_p) + 1.3K_eC_A/m_{KI}$$

where the denominator in their eq 9 is approximated as unity and K_p is a constant in the linear relation that usually applies to normal uncharged polymer systems

$$(S_{p'}^*)^{-1} = (S_{p'}^0)^{-1}(1 + 1.3nK_pC_A)$$

In notation of this paper:

$$1.3K_e = \frac{\theta^2 f_\pm Z^2 1.3}{2M_{p'}M(1-\bar{v}\rho)} = \frac{\theta^2 f_\pm \nu^2 N}{2 \times 1.3(1-\bar{v}\rho)}$$

where

$$f_\pm = (1/2)(f_{K^+} + f_{I^-}) \sim 2 \times 10^{-9}$$

Z is the valence of an AI polyion = $\nu n M_A = \nu M/1.3$, and $M_{p'}$ is the mass of an AI polyion. Thus $1.3K_e \sim 5 \times 10^8\theta^2$.

This estimate of the coefficient of C_A/m_{KI} taken from experimental conditions is equated to the value obtained from the slope of the line in Figure 5 to yield the result: $\theta^2 \sim 40$. Since by definition $0 < \theta < 1$, this result indicates that the Alexandrowicz and Daniel treatment is not valid for AI complexes.

References and Notes

(1) Presented in part at the Midwest Regional Meeting of the American Chemical Society, Iowa City, Iowa, November 7–8, 1974.
(2) For reviews of the complex see: (a) C. T. Greenwood, *Adv. Carbohydr. Chem.*, **11**, 367 (1956); (b) J. F. Foster, "Starch: Chemistry and Technology", Vol. I, R. L. Whistler and E. F. Paschall, Ed., Academic Press, New York, N.Y., 1965, Chapter XV; (c) H. Morawetz, "Macromolecules in Solution", Interscience, New York, N.Y., 1965; (d) J. Szejtli and S. Augustat, *Staerke*, **18**, 38 (1966).
(3) R. L. Whistler and C. Johnson, *Cereal Chem.*, **25**, 418 (1948).
(4) S. Lanzky, M. Kooi, and T. J. Schoch, *J. Am. Chem. Soc.*, **71**, 4066 (1949).
(5) J. F. Foster and D. Zucker, *J. Phys. Chem.*, **56**, 170 (1952).
(6) J. F. Foster and E. F. Paschall, *J. Am. Chem. Soc.*, **74**, 2105 (1952).
(7) K. H. Meyer and P. Bernfeld, *Helv. Chim. Acta*, **24**, 389 (1941).
(8) T. Kuge and S. Ono, *Bull. Chem. Soc. Jpn.*, **33**, 1269 (1960).
(9) K. Takahashi and S. Ono, *J. Biochem.*, **72**, 1041 (1972).
(10) B. Pfannemüller, H. Mayerhöfer, and R. C. Schulz, *Biopolymers*, **10**, 243 (1971).
(11) M. B. Senior and E. Hamori, *Biopolymers*, **12**, 65 (1973).
(12) K. O. Pedersen, *J. Phys. Chem.*, **62**, 1282 (1958).
(13) P. F. Mijnlieff, "Ultracentrifugal Analysis in Theory and Experiment", J. W. Williams, Ed., Academic Press, New York, N.Y., 1963.
(14) Z. Alexandrowicz and E. Daniel, *Biopolymers*, **1**, 447 (1963).
(15) T. J. Schoch, *Adv. Carbohydr. Chem.*, **1**, 247 (1945).
(16) W. W. Everett and J. F. Foster, *J. Am. Chem. Soc.*, **81**, 3460 (1959).
(17) F. R. Dintzis and R. Tobin, *Biopolymers*, **7**, 581 (1969).
(18) W. Banks, C. T. Greenwood, and D. D. Muir, *Staerke*, **23**, 118 (1971).
(19) A. C. Beckwith, H. C. Nielson, and R. O. Butterfield, *Anal. Chem.*, **43**, 1471 (1971).
(20) C. Tanford, "Physical Chemistry of Macromolecules", Wiley, New York, N.Y., 1961.
(21) J. W. Williams, K. E. VanHolde, R. L. Baldwin, and H. Fujita, *Chem. Rev.*, **58**, 715 (1958).
(22) R. Trautman, "Ultracentrifugal Analysis in Theory and Experiment", J. W. Williams, Ed., Academic Press, New York, N.Y., 1963.
(23) R. J. Goldberg, *J. Phys. Chem.*, **57**, 194 (1953).
(24) A. Savitsky and M. J. E. Goley, *Anal. Chem.*, **36**, 1627 (1964).
(25) J. A. Thoma and D. French, *J. Am. Chem. Soc.*, **80**, 6142 (1958).
(26) Z. Alexandrowicz and E. Daniel, *Biopolymers*, **6**, 1500 (1968).
(27) J. T. Edsall and J. Wyman, "Biophysical Chemistry", Vol. I, Academic Press, New York, N.Y., 1958, p 272.
(28) J. C. Thompson and E. Hamori, *Biopolymers*, **8**, 689 (1969).
(29) R. S. Higginbotham, *J. Text. Inst., Trans.*, **40**, 783 (1949).
(30) C. L. Cronan and F. W. Schneider, *J. Phys. Chem.*, **73**, 3990 (1969).
(31) R. E. Rundle and D. French, *J. Am. Chem. Soc.*, **65**, 1709 (1943).
(32) H. G. Elias and J. Gerber, *Makromol. Chem.*, **112**, 122 (1968).
(33) J. Gerber and H. G. Elias, *Makromol. Chem.*, **112**, 142 (1968).
(34) The mention of firm names or trade products does not imply that they are endorsed or recommended by the U.S. Department of Agriculture over other firms or similar products not mentioned.

Amylose–Iodine Complex. II. Molecular Weight Estimates[1]

F. R. Dintzis,* R. Tobin, and A. C. Beckwith

Northern Regional Research Laboratory, Agricultural Research Service, U.S. Department of Agriculture, Peoria, Illinois 61604.

Received May 8, 1975

ABSTRACT: Ultracentrifugation measurements made by the Archibald method on solutions of amylose–iodine–iodide (AI) complexes, containing 0.003% amylose of weight average molecular weight 4.0×10^5 at 3.6×10^{-3} M KI, yield an apparent molecular weight at the meniscus of 8×10^5 when measurements are extrapolated to 1200 rpm. Sedimentation equilibrium measurements at 1200 rpm yield apparent molecular weight at the meniscus of 6×10^5 and at the cell bottom of 2.4×10^6. Heterogeneity and aggregation are major features of AI complex solution behavior. Apparent molecular weights increase as a function of increasing potassium iodide concentration and with time. This behavior directly correlates with AI complex sedimentation coefficient behavior previously reported. Molecular weight estimates are of the same order for AI complex solutions saturated and 65–70% saturated with respect to the iodine-binding capacity of amylose. Qualitative estimates of net macroion charge effects upon apparent molecular weights are presented.

This paper continues a study of amylose–iodine–iodide (AI) complexes in very dilute solutions in which measurements are made on many of the same stock solutions for which sedimentation data were presented previously.[2] Molecular weight estimates from ultracentrifuge measurements were calculated mainly by the transient method of Archibald.[3] We report a few estimates based on sedimentation equilibrium measurements. The purpose of this paper is to obtain molecular weight estimates on AI complexes in solution and to determine whether or not the increase in sedimentation coefficient observed with increasing potassium iodide concentration represents aggregation.

Many practical and theoretical aspects of molecular weights determined with an ultracentrifuge are now well established and documented. An ample bibliography is provided by Creeth and Pain[4] in their useful general review. Because of the uncertainties that exist in our experimental data, we believe a detailed consideration of theory is not warranted. Therefore, data will be discussed qualitatively in terms of existing simple theory.

Theory

Molecular weights estimated from the transient method of Archibald are calculated by a conventional formulation for the upper meniscus:

$$\left(\frac{1}{rC}\frac{dC}{dr}\right)_{r=r_m} = \frac{M_{(r_m)}^{app}(1-\bar{v}\rho)\omega^2}{RT} \quad (1)$$

where C = count number, which is proportional to AI concentration and is measured with absorption optics; r = distance from center of rotation; r_m = distance from center of rotation to upper meniscus; $\bar{v}$ = partial specific volume of solute; ρ = density of solution; ω = angular velocity of rotor; R = gas constant; T = absolute temperature; and $M_{(r_m)}^{app}$, the apparent molecular weight at the meniscus, is expressed as: